Developing the active trap model for CCD charge transfer optimisation in large-scale space missions

Conference or Workshop Item

Developing the Active Trap Model for CCD charge transfer optimisation in large-scale space missions

T. W. Buggey[a], M. R. Soman[a], D. J. Hall[a], S. Parsons[a], N. Bush[a+b], O. Hetherington[a], G. Randall[a], M. Leese[a] and A. D. Holland[a]

[a]Open University, Centre for Electronic Imaging (CEI), STEM, Milton Keynes, United Kingdom, MK18 3FZ

[b]Jet Propulsion Lab, California Institute of Technology, 4800 Oak Grove Dr, Pasadena, CA91109, United States

ABSTRACT

Charge coupled devices (CCDs) have been the detector of choice for large-scale space mission for many years. Although dominant in this field, the charge transfer performance of the technology degrades over time due to the harsh space-radiation environment. Charge transfer performance can be optimized however, but it is often time consuming and expensive due to the many operating modes of the CCDs. A new technique is presented and developed here, which uses new measurements of the trap landscape present in a CCD, to predict changes in charge transfer inefficiency as a function of different variables. By using this technique, it is possible to focus experimental lab testing on key device parameters, potentially saving many months of laboratory effort.

Due to the generality of the method, it can be used to optimize the charge transfer performance of any CCD, and as such has many uses across a wide range of fields. Future CCDs variants that will be used in potential space missions (EMCCD and p-channel CCDs) can use this technique to feedback key device performance to the wider mission consortium before devices are available for experimental testing.

Keywords: Active Trap Model, CCDs, radiation-induced defects, trap pumping, trap landscape, space instrumentation

1. INTRODUCTION

For many years, Charge Coupled Devices (CCDs) have been the detector of choice for large space missions due to unparalleled energy resolution, noise performance and longevity in-orbit [8,9,10,11]. Although the technology has been dominant for many years, the charge transfer performance of the device is degraded by the harsh radiation environment present in space [12]. In order to deal with the issue of charge transfers losses, CCDs can be optimised to minimise charge transfer inefficiency (CTI) and hence maximise the lifetime of the devices. Full charge transfer optimisation pre-flight requires CCDs to be exposed to similar radiation conditions as seen in orbit, and are often irradiated at high-energy particle facilities most similar to the radiation environment they will operate in. Device performance is then assessed pre and post-irradiation and necessary optimisation activities can begin.

One recent characteisation test that has been developed, named trap pumping, allows the level of radiation damage within a CCD to be quantified to high precision. In particular, the technique allows the characterisation of displacement damage effects within the CCD, which must be fully understood to maximise charge transfer optimisation activities. Recent advances in knowledge of the distribution of defects through the trap pumping technique have led to key results that can be used to optimise CCDs fully. Figure 1 shows the emission time constant distribution of both intrinsic and radiation-induced defects in a CCD204, that was attained through the trap pumping technique as an example (black histogram). It is this distribution of defects that affects CCD charge transfer performance and has the potential to heavily degrade performance.

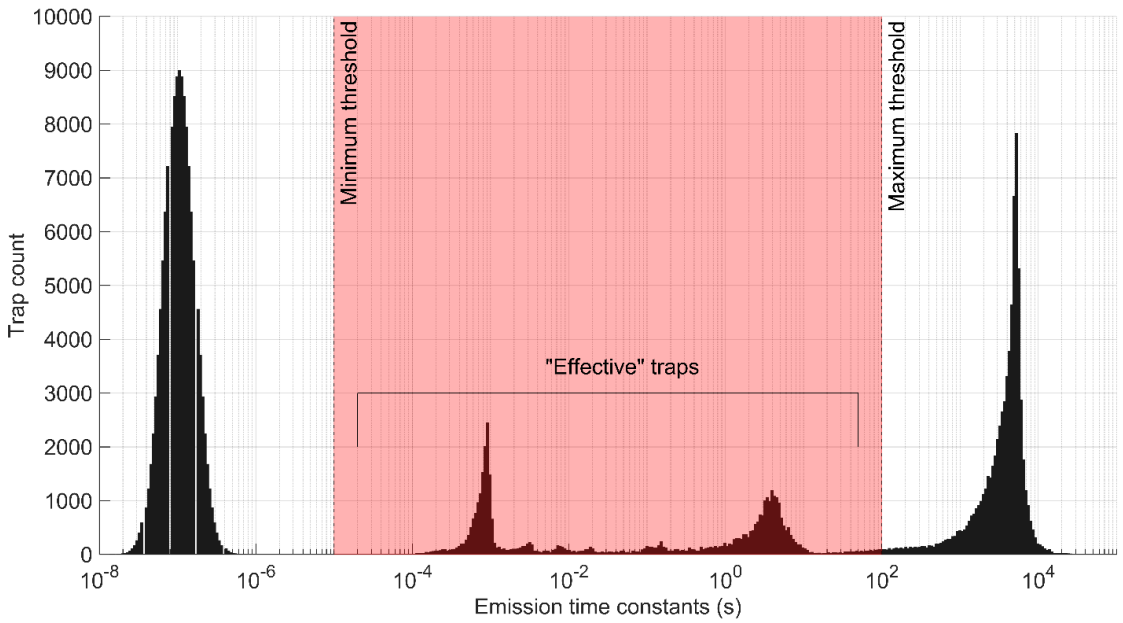

Figure 1: Room temperature trap landscape generated at 153K. A range defined by a minimum and maximum threshold is defined, showed in red. Any defects located within this range will contribute to CTI. [7]

However, due to the way the CCD is operated, not all of the defects present within the defect landscape in Figure 1 will contribute to charge transfer losses. To calculate which specific defects affect charge transfer performance a minimum and maximum threshold must be defined, with the defects between these limits causing CTI. If, for a specific of operating parameters, the thresholds can be clearly defined, then the charge transfer performance of the device can be estimated without measuring CTI directly.

Previous work utilised this optimisation method, known as the Active Trap Model, as part of the Nancy Grace Roman Space Telescope to optimise charge transfer performance of an Electron Multiplying CCD201 [1,2]. More specifically, a simple model was developed to optimise a single phase of readout for one operating mode (full frame readout) at a range of temperatures. However, CCD-based space missions are wide ranging, operating using different CCDs from different manufacturers (and hence different trap landscapes), at different clocking speeds and at different temperatures. Alternative readout modes such as a frame-transfer mode, opposed to the more simplistic full-frame readout mode are widely used also.

The Active Trap Model is powerful, as it can probe a wide parameter space in a very short space of time (~minutes compared to months of laboratory testing). However, the vast range of features above necessitate the development of the Active Trap Model, in order to be used on different CCD based space missions.

One such mission, the European Space Agency (ESA) mission SMILE, is a CCD based space mission that will utilize Te2v CCD370s operated in a frame-transfer mode with 6x6 on-chip binning. The complex readout nature of the devices, and associated experimental testing values, provide an excellent source of data to develop, test and modify the Active Trap Model.

This paper will describe the methodology behind the Active Trap Model, outlining each step of the technique and associated theory. After description of the model, experimental trap pumping results of a room-temperature irradiated CCD280 will be presented and then used as input to the Active Trap Model. Finally, X-ray CTI measurements of the CCD280 (as a function of temperature) will be compared to the output of the newly modified Active Trap Model.

2. ACTIVE TRAP MODEL METHODOLOGY

The Active Trap Model has several steps to correctly calculate the estimated number of effective traps (traps which contribute to CTI, between the minimum and maximum threshold in Figure 1) for a given devices operating mode. The method utilises trap landscapes attained previously, trap capture and emission dynamics as well as Shockley-Read-Hall (SRH) theory to calculate the probability that a filled trap will emit its captured electron in a given timeframe. Figure 2 shows a flowchart representing the stages of the analytical solution.

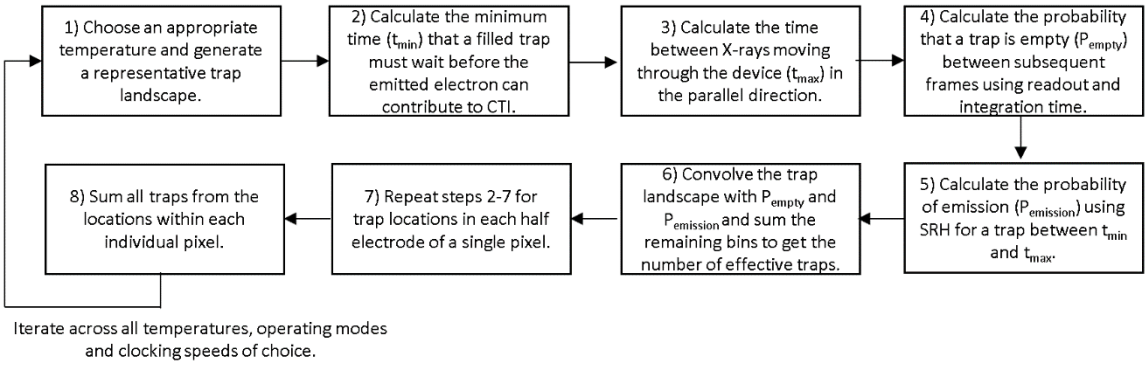

Figure 2: Flowchart showing the steps of the analytical solution to estimate the number of effective traps that will degrade CTI in a specific device and readout mode.

2.1 Generating initial trap landscapes

To correctly estimate the effective number of traps, the most representative initial trap landscape must be used with respect to both irradiation conditions and fluence alongside the operating temperature. Using either a room-temperature (RT) or cryogenically irradiated landscape ensures that the correct distribution of traps is present when comparing the number of effective traps to a CTI value. The correct operating temperature ensures that the emission time constants are located in the correct position within the trap landscape. Figure 3 shows the same RT landscape generated at three different temperatures. As temperature increases, the entire landscape shifts to a faster emission time constant, while still retaining the same distribution.

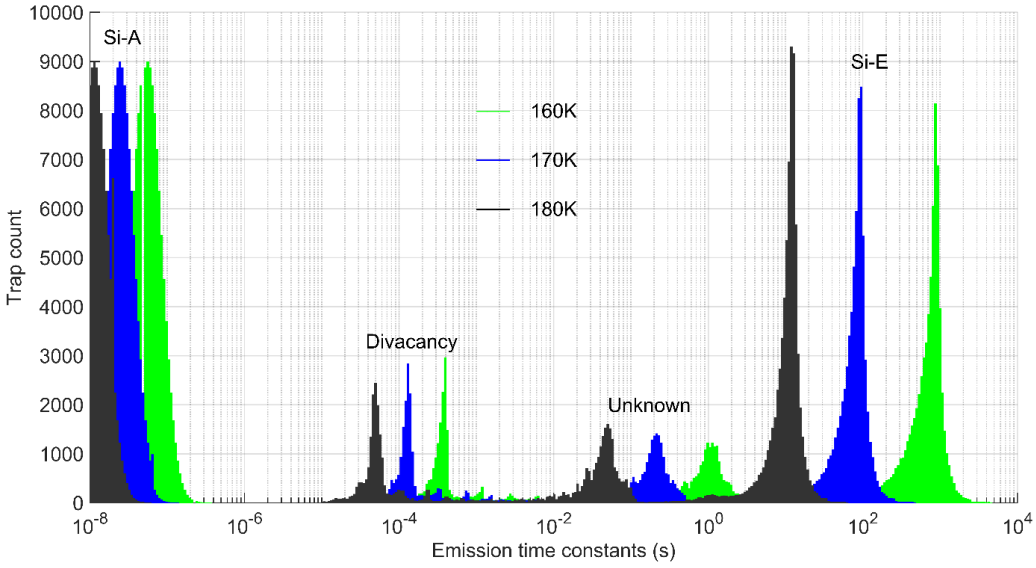

Figure 3: Generated trap landscapes for a CCD204 at three temperatures, with the main radiation-induced defects highlighted for clarity.

2.2 Calculating the lower time threshold for effective traps

The minimum timing defines the trap with the quickest emission time constant that can contribute to CTI and hence be counted as an effective trap. Any traps with a quicker emission time constant than the minimum timing will emit back into the source charge packet and will not contribute to CTI. In terms of device performance, the minimum timing value originates from the timings within the device in question, namely the parallel and serial clocking speeds.

Previous work calculated the minimum timings for traps within each electrode of a single pixel separately but assumed that the trap position within the electrode was irrelevant [1,2]. Figure 4 (left) shows this whole-electrode approach outlined specifically for a four-phase CCD. Charge is moved sequentially from phase one through to four, with the serial register readout in stage one. The total time for each stage of the transfer process is indicated by the time y-axis. Using this diagram, it is possible to calculate the minimum time that a filled trap must wait before emission can occur into a non-source charge packet and be classified as an effective trap that contributes to CTI.

Defects present under phase one fill during stage one of the transfer process. Once charge capture occurs, emission can occur and potentially contribute to CTI. As charge moves to phase two, any emission that occurs will mean that the captured electron re-joins the source charge packet as the source charge packet is still the closest charge packet. When the charge packet moves to electrode three, the whole-electrode approach now faces a complication, as both the succeeding and source charge packet are equidistant from the filled trap. This means that it is not clear whether the time taken for stage three (t_{image}) should be included when calculating the lower limit time threshold.

2.3 Sub-electrode modelling

This issue can be ameliorated by instead considering defects within each half electrode, as seen in Figure 4 (right). Analysing the emission of defects under phase one once again, defects under the left-hand-side (LHS) of electrode one emit into the non-source packet and thus the time taken for this stage of transfer is not included in the minimum threshold time. On the other hand, defects on the right-hand-side (RHS) of electrode one are closer to the source charge packet and thus when emission occurs, emission does not contribute to CTI. This means that the time taken for stage three **is** included in the minimum threshold time.

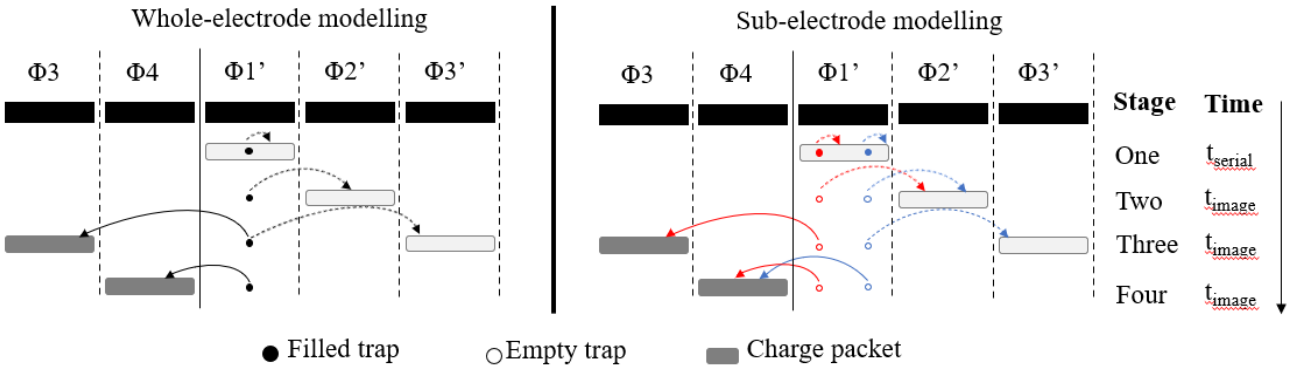

Figure 4: Trap emission dynamics for a four-phase CCD using the whole-electrode or sub-electrode modelling approach. Note that the dashed and solid lines represent emission back into the source and non-source charge packet respectively. Also note that for the whole-electrode modelling, the defect is assumed to be in the centre of the electrode.

By repeating the procedure for each half electrode, it is possible to precisely calculate the minimum threshold time. Table 1 summarises the minimum threshold times calculated for trap positions in both the whole-electrode and sub-electrode model. Due to the uncertainty of the trap emission dynamics within the whole-electrode model, the whole-electrode model cannot precisely predict the minimum threshold timing. This contrasts with the sub-electrode model, which more precisely calculates the minimum threshold timing.

Table 1: Minimum threshold timings calculated for both the whole-electrode (WE) and sub-electrode (SE) modelling. Note that the whole-electrode minimum timing is identical for both trap positions within the electrode as the electrode is not sub-divided into halves.

Electrode	Trap position within electrode	WE model $t_{minimum}$	SE model $t_{minimum}$
1	Left	$t_{serial} + t_{image}$ *or* t_{serial} $2t_{image}$	$t_{serial} + t_{image}$
1	Right	$t_{serial} + t_{image}$ *or* $t_{serial} + 2t_{image}$	$t_{serial} + 2t_{image}$
2	Left	2_{image} *or* 3_{image}	$2t_{image}$
2	Right	$2t_{image}$ *or* $3t_{image}$	$3t_{image}$
3	Left	$2t_{image}$ *or* $3t_{image}$	$2t_{image}$
3	Right	$2t_{image}$ *or* $3t_{image}$	$2t_{image} + t_{serial}$
4	Left	$3t_{image}$ *or* $3t_{image} + t_{serial}$	$t_{image} + t_{serial}$
4	Right	$3t_{image}$ *or* $3t_{image} + t_{serial}$	$t_{serial} + 2t_{image}$

The main issue with using the approximate whole-electrode model is the difference between t_{image} and t_{serial} timings, with approximate values shown in Figure 5. The time to readout the serial register (t_{serial}) is significantly longer than the parallel timing (t_{image}), meaning that the window for the effective number of traps is significantly reduced. Any electrode position when the t_{serial} is included in the minimum timing threshold will greatly affect the number of effective traps estimated by the analytical model. This means that the sub-electrode model must be used in order to accurately calculate the minimum threshold time, as the whole-electrode model miscalculates the contribution from the image and serial timings respectively.

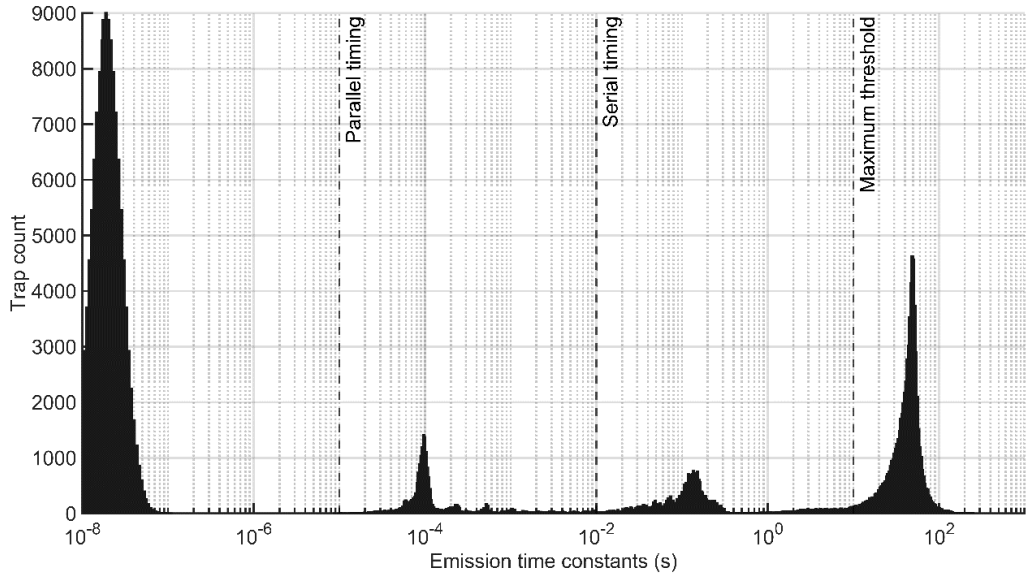

Figure 5: Trap landscape showing the maximum threshold along with two minimum thresholds, namely the parallel and serial timing.

2.4 Calculating the time between X-rays (Upper limit of effective traps)

Once the minimum threshold is calculated, the next stage of the analytical solution is to calculate the maximum threshold. This boundary defines the slowest trap that will be counted as an effective trap and contribute to CTI, any defects that have an emission time constant slower than the upper threshold will not be counted as an effective trap. Physically, this value is defined by the presence of additional charge, either in the form of X-rays often used to measure CTI or supplemental charge injection (often used to reduce CTI). The density of X-rays or number of lines of charge injection has a direct effect on the location of the upper threshold.

As this external charge is moved through the device, it passes over defects, filling them as it moves. If a defect is filled, it cannot capture additional charge and is thus effectively suppressed with respect to degrading CTI. If a higher X-ray density is present, this means that X-rays pass over defects more frequently, lowering the time between X-rays. As a result, the maximum threshold is lowered, and traps with a faster emission time constant are now suppressed.

2.5 Probability of empty traps

For a trap to contribute to CTI, it must capture charge from a charge packet and then emit this charge back into the non-source charge packet. This means that the trap must first be *empty*, or charge capture cannot occur, and the trap cannot contribute to CTI. For a fully physical and representative analytical model, this means that the proportion of traps that are empty/full must be calculated.

To be able to calculate the proportion of traps that are empty (and can contribute to CTI) both the readout speed and integration time used in the X-ray CTI data must be taken into account. When X-ray CTI data is collected, many frames are often read out to ensure that an X-ray spectrum can be seen above the detector noise. This means that between frames, traps emit their captured charge and are thus empty to capture charge for the next X-ray CTI frame.

2.6 Calculating the probability of emission and empty probabilities

Once the minimum and maximum times have been calculated for different locations within each pixel, the probability that a trap will emit within these two timings can be calculated via SRH with Eq.1, starting with the general form for emission between times t_1 and t_2:

$$\text{Probability of emission} = \exp\left(\frac{-t_1}{\tau_e}\right) - \exp\left(\frac{-t_2}{\tau_e}\right) \qquad \text{Eq.1}$$

Substituting $t_1 = t_{min}$ and $t_2 = t_{max}$ leads to the expression for the probability that traps of emission time constant τ_e will emit between the times of t_{min} and t_{max} (Eq.2).

$$\text{Probability of emission} = \exp\left(\frac{-t_{min}}{\tau_e}\right) - \exp\left(\frac{-t_{max}}{\tau_e}\right) \qquad \text{Eq.2}$$

Similarly, the probability of a trap emptying between frames is given by the equation:

$$\text{Probability of empty traps} = 1 - \exp\left(\frac{-t_{r+int}}{\tau_e}\right) \qquad \text{Eq.3}$$

Where t_{r+int} is the time to readout a single frame plus the integration time and t_1 is set to zero.

Once calculated, the probability of emission and probability of empty traps can be used in combination with the trap landscape to calculate the total number of effective traps. A graphical representation of the trap landscape and associated probability functions are shown in Figure 6.

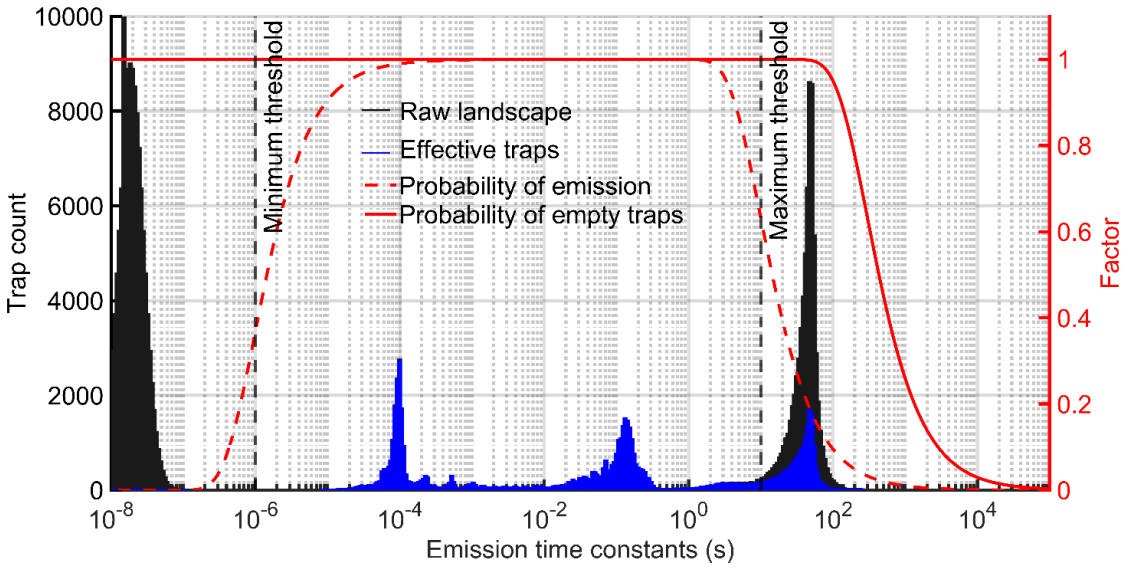

Figure 6: Raw trap landscape from an irradiated CCD204 in black. The effective trap landscape is shown in blue which is attained by convolving the raw trap landscape with the two red probability functions.

The black distribution in Figure 6 represents the total defects within an irradiated CCD204 and the left y-axis shows the total trap counts. The probability of emission and probability of empty traps are represented by the red dashed and solid line respectively and are associated with the right y-axis. A factor of one represents a 100% probability of emission and 100% probability of a trap being empty. Alternatively, a factor of 0 represents a 0% chance of emission and a filled trap.

To calculate the effective number of traps (blue distribution) the raw landscape (black distribution) is convolved with both the probability of emission and probability of empty traps. In the example of Figure 6, it is clear that the timings used within the analytical model affect different parts of the landscape in regard to the number of effective traps. For example, the effective trap contributions from the Si-E are suppressed due to the maximum threshold timing lowering the probability of emission of the majority of the Si-E. This is shown explicitly by the difference in peak height of the Si-E for the raw and effective traps landscape, respectively.

For the area containing the divacancy and unknown defect, the timings used within the device mean that 100% of the defects between ~1 × 10^{-4}s and 1s emit and contribute to the effect number of traps, once again explicitly shown by the identical height of both the raw and effective trap landscape in this region.

3. GENERATING A REPRESENTATIVE TRAP LANDSCAPE

As mentioned in section 2.1, the trap landscape used as input to the Active Trap Model must be representative of the device which is being compared, in this case the CCD280 irradiated at room-temperature. This necessitates the use of the trap pumping technique, which will be outlined in the section below.

3.1 Trap pumping technique

To probe the defects within the silicon, both pre and post irradiation, the trap pumping technique is used [1,2,3,4]. The technique allows the emission time constants of the intrinsic and radiation-induced defects to be calculated, which can then be collated to provide an overall representation of the spread of emission time constants.

The trap pumping technique relies upon the rapid, sequential movement of charge through a designated area of the device. A known number of electrons is added to a selected number of pixels in the device, often via the charge injection

method. Once added, different trap pumping schemes are used to probe different areas of each pixel. Figure 7 shows the 1-2-3-2-1 trap pumping scheme, with charge initially stored under Φ1. Defects under this phase initially capture electrons, as seen by the filled red circles. After a time t_{ph}, charge is moved to Φ2 and the captured charge is now free to emit. The released electron joins the closest charge packet, which is still the source charge packet, so there is no net movement of charge (indicated by the dashed arrows). Whether the defect is in the left- or right-hand side of Φ1 is irrelevant, both defect locations are still closest to the source charge packet and hence there is still no net movement of charge. The pumping sequence continues, with charge now moved into Φ3. Defects under Φ1 can still be filled by captured electrons (depending on their emission time constant) and will still emit into the closest charge packet. For the case of defects on the right-hand side of Φ1, the closest charge packet is still the source charge packet, so once again no net movement of charge is seen. However, defects located in the left-hand side of Φ1 are now closest to the charge packet in the adjacent pixel, with emitted electrons now joining this non-source charge packet (indicated by the solid black line in Figure 7). Overall, this means that an electron has been moved, or "pumped", from the pixel enclosed by the blue dashed line, into an adjacent pixel, from a single pump cycle.

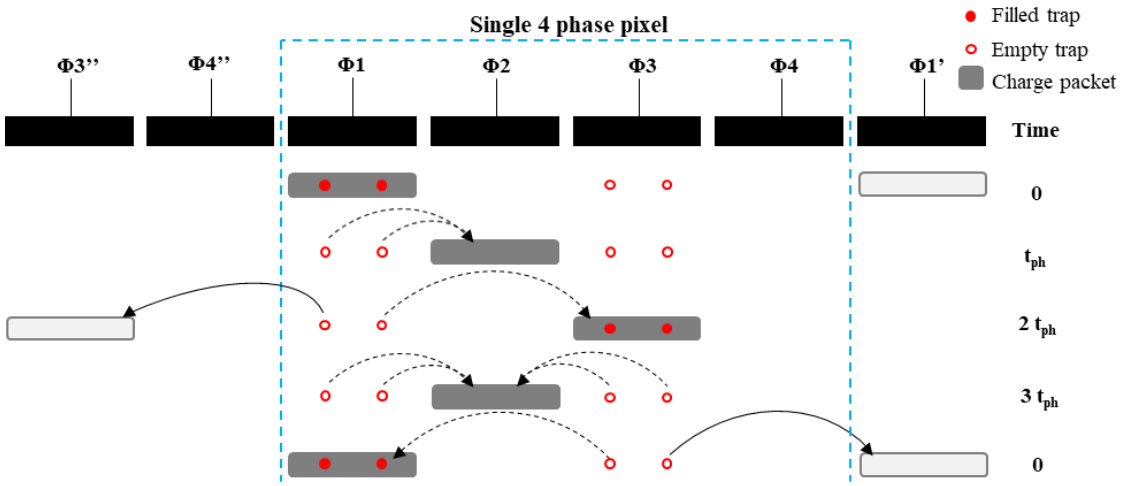

Figure 7: Defect capture and emission dynamics for a single trap pumping cycle as part of the 1-2-3-2-1 trap pumping scheme. Note that dashed and solid black arrows represent emission into the source and non-source charge packet respectively.

When the trap pumping schemes are implemented, utilizing up to 10,000 pump cycles, distinct patterns of signal are seen within each trap pumped image, shown in Figure 8 (left). Each trap probed is revealed by two adjacent pixels (in the row direction) showing a contrast of high and low signal, named charge dipoles. By analyzing each column in each image (Figure 8 right) it is possible to locate each trap and proceed with the next stage of analysis.

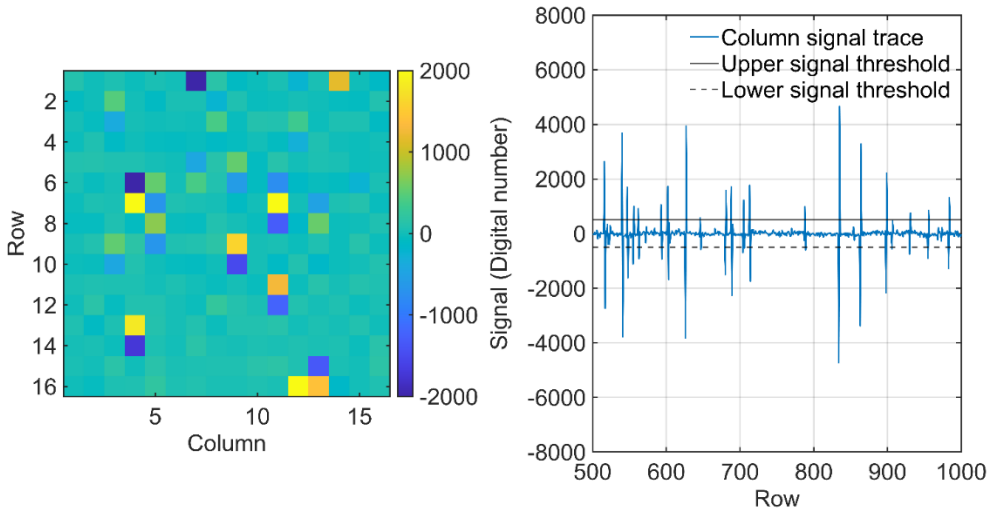

Figure 8: Charge dipoles that are visible after a background signal subtraction (left). Note that the orientation of the dipoles is not consistent, suggesting that some defects are located in different sub-phase locations within each pixel. Right - Changing pixel signal as a function of row number across a single image column, with the upper and lower limit for dipole selection shown.

For each defect, the signal of the charge dipole is plotted as a function of the parallel pumping delay (t_{ph}), and shows a characteristic smooth curve as seen in Figure 9.

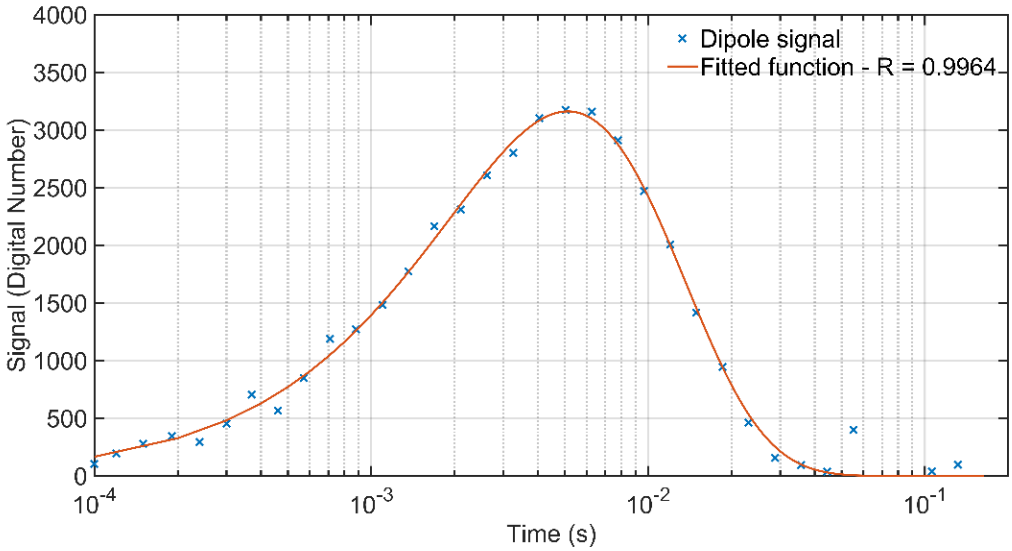

Figure 9: Characteristic dipole intensity curve (blue crosses) with the fitted function overlaid (red line). Once fitted, defects are down selected, with fits of R < 0.9 rejected.

By fitting the equation relevant (Eq.4) to the specific trap pumping scheme used, both the emission time constant as well as the probability of capture can be attained.

$$I = NP_p = NP_c\left(\exp\left(\frac{-t_{ph}}{\tau_e}\right) - \exp\left(\frac{-2t_{ph}}{\tau_e}\right)\right) \qquad \text{Eq.4}$$

Once defects across the whole parameter space are fitted and down selected, the emission time constants are binned into a histogram, representing the spread of emission time constants within the parameters space proved.

3.2 Results from a room-temperature irradiated CCD280

As part of the CCD280 post-irradiation characterization, a trap pumping sweep was planned, targeting the main defects of interest, namely the double negative state of the divacancy and the unknown defect. Figure 10 shows the four main, radiation-induced defects that can affect N-channel CCD charge transfer performance, with the emission time constants ranges probed shown as black vertical lines.

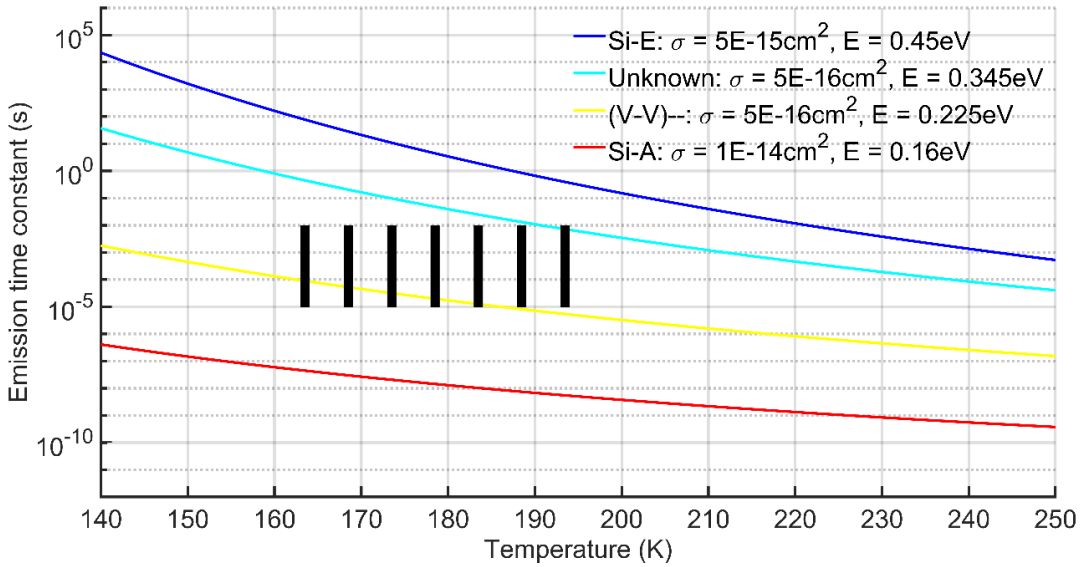

Figure 10: Trap diagram showing the four most abundant radiation-induced defects relevant to N-channel charge transfer performance [5]. Overlaid are the six trap pumping sweeps planned, focusing on the double negative state of the divacancy, the unknown defect, and the emission time constant range between these two defects.

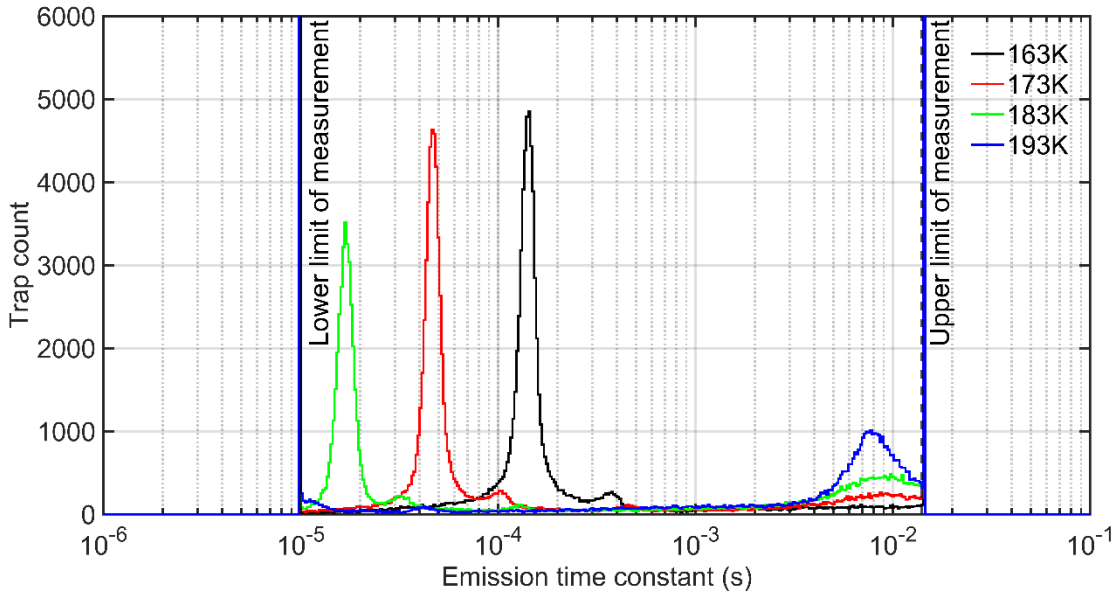

Figure 11: Trap landscapes directly measured in the CCD280 post-irradiation. The lower and upper limit of measurement are defined by the parallel clock speed and time allocation for this phase of characterisation, respectively.

To generate as complete a CCD280 landscape as possible, the landscapes containing the divacancy and unknown (Figure 11) can be combined to form an overall landscape, with this landscape used as input to the Active Trap Model. To combine the trap landscapes, the known literature values for the energy level and cross section of both the divacancy and unknown defect can be used [6], in combination with SRH, to shift the emission time constant of both landscapes. Figure 12 shows the original trap pumping data (top) with the combined and temperature corrected data beneath.

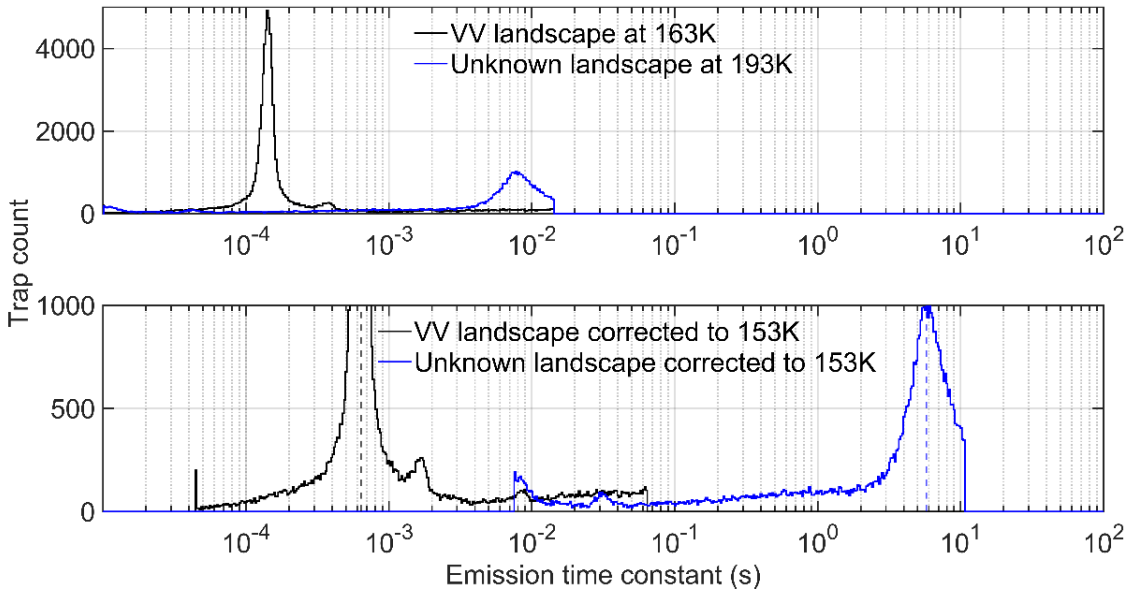

Figure 12: Original trap pumping data (top) along with the temperature corrected landscape below. The black and blue dashed line represent the known peak emission time constants of the divacancy and unknown respectively.

Figure 12 (bottom) shows the distribution of emission time constants for both temperature-corrected landscapes, with the peak of the divacancy and unknown defect aligning with the known literature values [6]. However, it can be seen that there is some overlap between the two landscapes, as although different temperatures were used to probe both the divacancy and unknown (163K and 193K respectively), some overlap in emission time constant is still present. This is shown most explicitly by the presence of the small peak visible in both the divacancy corrected landscape (8.5×10^{-3} s) and unknown corrected landscape (3×10^{-2} s).

Utilising the known literature values of the divacancy and unknown defect to temperature-correct the landscape does work (as seen by Figure 12 (bottom)), however this does not necessarily mean that the remainder of the trap landscape is situated at the correct emission time constant. The reason for this discrepancy is the use of log-spaced bins which is necessary given the wide range of emission time constants probed. As you move away from the corrected peak values, the inaccuracy increases, and the two landscapes do not align as expected.

To ameliorate the issue, the average of number of defects located between the emission time constant values of 7.5×10^{-3} s and 6.3×10^{-2} s for both the divacancy and unknown can be used to create a complete landscape. Although this is not a completely physically correct landscape, the distribution of defects between these two points is relatively flat and not dominated by a known abundant defect (such as the divacancy, unknown or Si-E).

3.3 Final landscape

Although a representative trap landscape has been constructed from experimental values, the emission time constants probed did not include the Si-E defect, and hence this abundant defect is not present. The defect is well studied however, with a known cross section and energy level. As a result, the defect can be added artificially to the landscape via the use of SRH to calculate the emission time constants of the Si-E, with the shape of the peak being estimated by a gaussian function. Although the position and shape of the Si-E peak can be added accurately, the defect density is less known. Figure 13 shows the trap landscape in Figure 12 (bottom) with the Si-E peak added with varying peak heights.

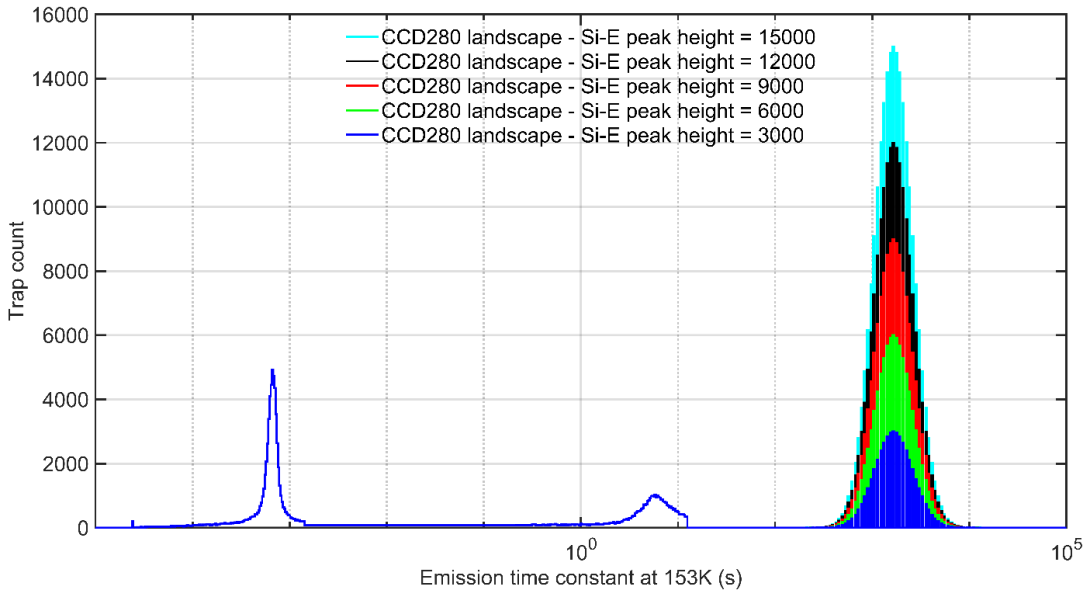

Figure 13: CCD280 trap landscape with a gaussian shaped Si-E peak added based upon known literature energy level and cross section values [6]. Gaussians with differing peak heights are shown here, that will subsequently be used an input to the analytical model.

The landscape in Figure 13 will be used as the input trap landscape to the Active Trap Model, with the peak height of the Si-E set as a range of parameters, to examine how the output result from the model varies.

4. RESULTS

To accurately compare predictions from the Active Trap Model to experimentally measured X-ray CTI values, the parameters used to collect laboratory data must be used in the Active Trap Model. Table 2 summarises the parameters used both in the collection of X-ray CTI and input parameters to the Active Trap Model.

Table 2: Experimental parameters used as input to the Active Trap Model.

Parameter	Value
Image line transfer time (s)	58×10^{-6}
Serial clocking speed (kHz)	50
Operating temperature (K)	143 - 188
Input trap landscape (Room temperature or cryogenic)	Room temperature (CCD280)
Serial register elements	1500
Integration time (s)	300
X-ray density (per raw pixel)	1/110

4.1 CTI vs effective traps as a function of temperature

Figure 14 shows the explicit comparison between the output of the Active Trap Model (right hand axis) and the X-ray CTI (left hand axis) measured for the CCD280 (irradiated at room-temperature). Both axis have been normalised to 143K to compare the rate of change of effective traps and CTI as a function of temperature. At low temperatures, the model and experimental data show excellent agreement up to ~165K for all Si-E trap densities, suggesting that at this temperature range, the Si-E defect does not play an important role in CTI. This is expected, as at this temperature range, the emission time constant of the Si-E is between 100 – 1000s (as seen in Figure 10), whereby it cannot empty fast

enough to contribute to parallel CTI transfers at ~ 1×10^{-6} s and it is filled by the relatively high X-ray density (1/110 pixels).

As temperature increases however, the predicted Active Trap Model values change significantly as a function of Si-E density. This is also expected, as the emission time constant of the Si-E has decreased enough, that when combined with the high trap density, the Si-E defect is dominating the total number of effective traps predicted by the Active Trap Model.

The Si-E defect density which predicts the best agreement between the Active Trap Model and the experimental X-ray CTI values is between a peak height of 15000 and 18000. Outside of this peak height range the model significantly under/overestimates the number of effective traps as a function of temperature. Although a peak height of between 15000 and 18000 shows a good fit across the whole temperature range, without comparisons to previous known defect densities, it is hard to comment further on the physical nature of the Si-E.

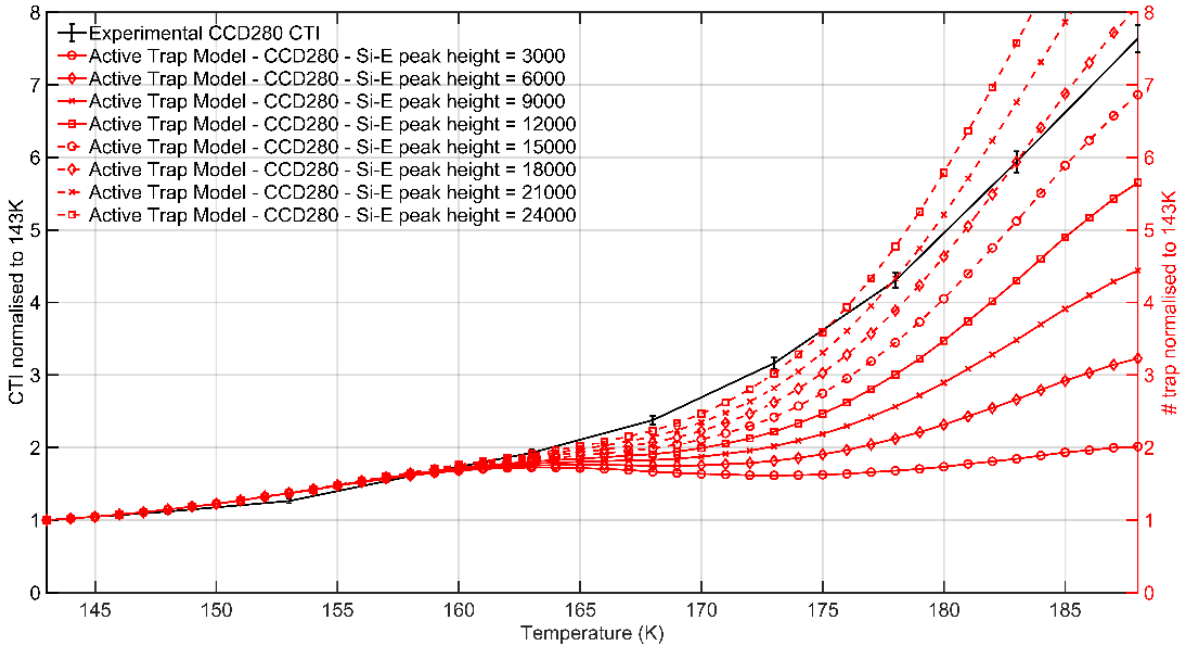

Figure 14: Comparison of X-ray CTI data and the Active Trap Model predictions as a function of temperature and Si-E peak height.

Fortunately, the trap landscape of the CCD204, shown in Figure 6, shows the defect density of the Si-E which can be used to compare defect densities. Directly comparing landscapes is difficult however, as many differences arising from device manufacturing and trap pumping parameters can skew the number of defects shown in both landscapes. To avoid these problems, *relative* contributions of defects in individual landscapes can be compared to each other. That is, comparing the peak density of the double negative state of the divacancy (a stable defect at room-temperature) to the peak density of the Si-E, between both the CCD204 and CCD280 room-temperature irradiated landscape can give a good indication that the physically correct trap densities are used.

Table 3: Summary of the ratios between the divacancy and Si-E peak defect densities in the CCD204 landscape (Figure 6) and the constructed CCD280 trap landscape (Figure 13).

Device landscape	Divacancy peak density	Si-E peak density	Ratio of Si-E to divacancy
CCD204	~2700	~8700	**3.22**
CCD280 (15000 Si-E peak height)	~5000	~15000	**3**
CCD280 (18000 Si-E peak height)	~5000	~18000	**3.6**

Table 3 shows a summary of the ratios of the Si-E and divacancy defect in the two room-temperature irradiated trap landscapes currently available to the author. The ratios are similar, showing the relative concentrations of the divacancy and Si-E are physically correct (to current knowledge), while Si-E defect densities in the CCD280 landscape (15000 and 18000) provide the best agreement between experimental X-ray CTI results.

5. CONCLUSIONS AND FUTURE WORK

The Active Trap Model was described, with modifications added (sub-electrode modelling) in order to more accurately predict CCD charge transfer performance. Experimental data was acquired from a room-temperature irradiated CCD280, namely X-ray CTI and trap pumping data at a range of temperatures. Using the trap pumping data and subsequent analysis, a representative trap landscape was created, including the Si-E defect at a range of densities.

The Active Trap Model was then used to predict charge transfer performance of a CCD280, with the results explicitly compared to measured X-ray CTI. The Active Trap Model accurately predicts charge transfer performance of a CCD280 as a function of temperature, using a physically representative Si-E defect density.

With the basic physics of the updated Active Trap Model now validated versus experimental data, the model can be used to explore the performance of more sophisticated device clocking modes. More specifically, the charge transfer performance of a frame-transfer CCD with 6x6 on-chip binning (SMILE CCD370) as well as the potential benefit of tri-level clocking.

6. REFERENCES

[1] N. Bush, D. Hall, R. Burgon, A. Holland, D. Jordan. “Improving charge transfer performance within irradiated EMCCDs”. Proc. SPIE 10709, High Energy, Optical, and Infrared Detectors for Astronomy VIII, 1070913 (10 July 2018); doi: 10.1117/12.2313574

[2] “Optimisation of charge transfer in electron multiplying CCDs through use of an Active Trap Model” [in prep], N. Bush, D. Hall, T. Buggey, A. Holland.

[3] D. J. Hall, N. J. Murray, A. D. Holland, J. Gow, A. Clarke, D. Burt, “Determination of in situ trap properties in Charge Coupled Devices using a single-trap ‘ pumping ’ technique,” *IEEE Trans. Nuc. Sci*, **61**(4) p1826, 2014.

[4] Wood, Daniel (2018). Radiation-induced Deep-level Defects in CCD Imaging and Spectroscopy Sensors. PhD thesis The Open University.

[5] Bush, Nathan L. (2018). The Impact of Radiation Damage on Electron Multiplying CCD Technology for the WFIRST Coronagraph. PhD thesis The Open University.

[6] P. Pichler, “Intrinsic Point Defects, Impurities, and their Diffusion in Silicon”, *Springer*, 2004.

[7] N. Bush, B. Dryer. A, Lindley-DeCaire. “P-Channel CCD performance characterisation and radiation testing”, OU-PCHAN-FP-1-Iss1-Rev0, Issue 1, January 2018.

[8] Strüder, L., Briel, U., Dennerl, K., et al. 2001, A&A, 365, L18

[9] Weisskopf M. C. Brinkman B. Canizares C. Garmire G. Murray S. Van Speybroeck L. P.2002, PASP, 114, 1

[10] Windhorst, R. A., Cohen, S. H., & Hathi, N. P. et al. 2011, ApJS, 193, 27

[11] Perryman M. A. C.et al. 2001a, A&A, 369, 339

[12] Janesick, J., Elliott, T. and Pool, F.: 1989, 'Radiation damage in scientific charge-coupled devices',*IEEE Trans on Nuclear Science*,36, 572.